

Identifying the Ground State Geometry of a MoN₂ Sheet through a Global Structure Search and Its Tunable p-Electron Half-Metallicity

Cunzhi Zhang,[†] Junyi Liu,[†] Haoming Shen,[†] Xin-Zheng Li,[§] and Qiang Sun^{*,†,‡}

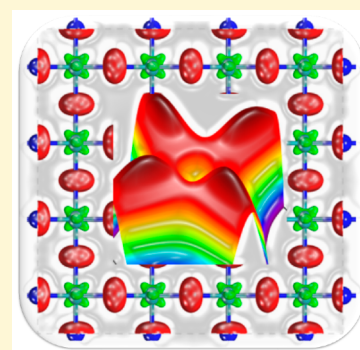
[†]Department of Materials Science and Engineering, COE, Peking University, Beijing 100871, China

[‡]Center for Applied Physics and Technology, Peking University, Beijing 100871, China

[§]International Center for Quantum Materials, School of Physics and Collaborative Innovation Center of Quantum Matter, Peking University, Beijing 100871, China

Supporting Information

ABSTRACT: MoN₂ and MoS₂ sheets are representatives of two-dimensional transition metal dinitrides and dichalcogenides, respectively. Their similarity in atomic ratios misled people to make an incorrect assumption in previous studies that the former adopts the geometry of the latter. However, compared with S, N is smaller and has fewer valence electrons, and N is more effective in mediating magnetic couplings; therefore, a different geometry and different properties can be expected for the MoN₂ sheet. Here using a global structure search, for the first time we have identified the ground state geometry of this sheet named Tetra-MoN₂ that is much more stable than the H phase proposed previously. Different from the metallic nature of H-MoN₂, Tetra-MoN₂ is a semiconductor having an indirect band gap of 1.41 eV with a flexible strain tunability. In particular, Tetra-MoN₂ can exhibit rich half-metallic behaviors mediated by the polarized p electron of N and induced by low-concentration hole doping and small strains that are readily achievable experimentally.



INTRODUCTION

Since the discovery of monolayer graphene,¹ many other two-dimensional (2D) crystals such as silicene,^{2,3} MoS₂,^{4,5} black phosphorus,^{6,7} etc., have been synthesized, displaying novel properties and promising applications. These advances greatly stimulated researchers to explore other new 2D materials with desirable properties. Among them, metal dinitride sheets have attracted special attention.⁸ Recently, the bulk crystal of MoN₂ was experimentally synthesized,⁹ based on this the MoN₂ monolayer was expected to exist and was predicted theoretically to exhibit a robust ferromagnetism with a Curie temperature of >420 K,¹⁰ and the magnetic coupling [ferromagnetic (FM) vs anti-ferromagnetic (AFM)] in the MoN₂ sheet can be further modulated through applied strain.¹¹ Moreover, monolayer MoN₂ was also found to be a promising material for battery electrodes with a high storage capacity.¹² These findings encouraged researchers to extend the study from the proposed H phase to other phases such as the T and T' phases¹³ or from Mo to other metal elements.^{14,15} However, recent studies questioned the stability of the MoN₂ monolayer in the H-phase configuration. A global structure search found a new non-layered ground state for the bulk MoN₂ system with N–N bonding at pressures ranging from atmospheric pressure to 82 GPa, while layered MoS₂-type MoN₂ has a high positive enthalpy of formation, a large imaginary frequency, and a negative C₄₄,¹⁶ suggesting that it is unstable thermodynamically, dynamically, and mechanically. Moreover, monolayer H-MoN₂ was also predicted to be unstable, and surface hydrogenation is required to maintain its stability.¹⁷ Hence, determining the

ground state geometry of the MoN₂ sheet and its physical properties is highly desirable.

Here we use a global structure search method¹⁸ and first-principle calculations to answer these two questions. A new structure with a tetragonal lattice (termed Tetra-MoN₂) is identified with an energy much lower than that of H- and T-MoN₂.¹³ Its dynamical and thermal stabilities are confirmed by calculated phonon spectra and by performing *ab initio* MD simulations (1000 K). Moreover, Tetra-MoN₂ is found to be an intrinsic semiconductor with an indirect band gap of 1.41 eV (at the HSE06 level). Because of flat top valence band and large exchange interaction, doping-induced magnetic properties are also investigated. It is found that the ferromagnetism in Tetra-MoN₂ can be induced at a carrier density of >1.25 × 10¹⁴ cm⁻², and when Tetra-MoN₂ is slightly strained ($\epsilon = 2\%$ and $\epsilon = 4\%$), half-metallicity can be induced by hole doping where the spin moments come mainly from the polarized p electrons of N. These findings can be well understood using the following arguments. (1) N has fewer valence electrons than S does, and a structural transition can be expected due to Jahn–Teller-like distortion. (2) The exchange interaction of nitrogen is larger than that of sulfur, which is conducive for spontaneous spin polarization. (3) Compared with sulfur, nitrogen is more effective at mediating magnetic couplings. For example, Mn₂ is an antiferromagnetic dimer that becomes ferromagnetic when

Received: April 19, 2017

Revised: September 19, 2017

Published: September 19, 2017

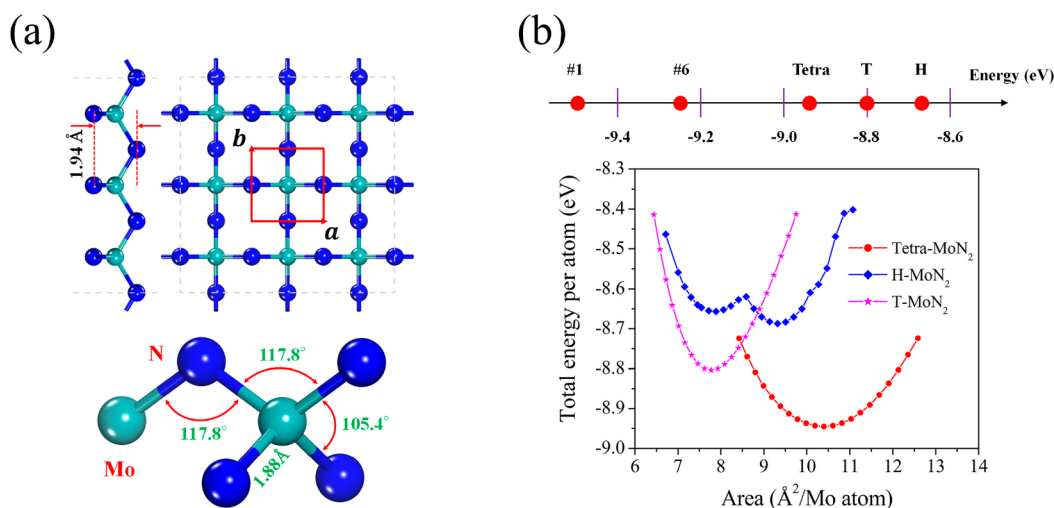


Figure 1. (a) Atomic structure of the Tetra-MoN₂ monolayer. (b) Comparison of the total energy per atom between MoN₂ isomers (#1 and #6 are bulk decomposed structures from ref 16) (top) and energy vs area per Mo atom for H-, T-, and Tetra-MoN₂ (bottom).

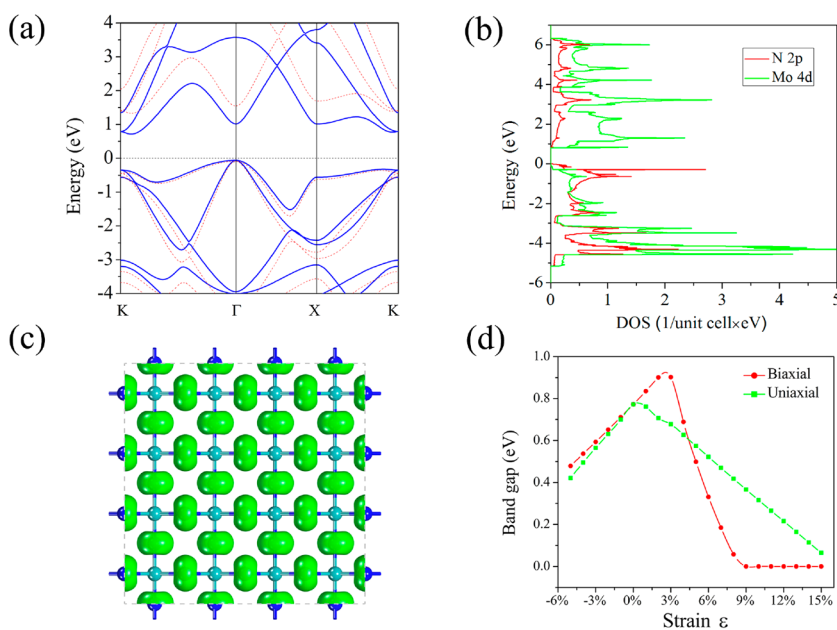


Figure 2. (a) Calculated band structure: (solid lines) PBE and (dashed lines) HSE06. (b) Orbital-projected density of states for N and Mo. (c) Band decomposed charge density distribution of the top valence band in panel a. (d) Band gap variation under biaxial and uniaxial strain (at the PBE level).

N is introduced,¹⁹ whereas Mn₂ remains antiferromagnetic when S is inserted;²⁰ when S atoms are replaced with N in the Ni₃C₁₂S₁₂ sheet, the Curie temperature can be significantly increased.²¹

COMPUTATIONAL METHODS

The atomic structure of the 2D Tetra-MoN₂ sheet is predicted using the PSO algorithm implemented in the CALYPSO package.¹⁸ The population size and the number of generations are set to be 30 to ensure convergence. The number of formula units per unit cell is set to be 1–4, corresponding to 3, 6, 9, and 12 atoms. To accommodate the buckling of the structure, the buffering thickness is set to 0.8 Å. Structural relaxation, total energy, and electronic property calculations are mainly performed by using Vienna *Ab initio* Simulation Package (VASP) based on density functional theory (DFT).²² The projector augmented wave (PAW) method is used to treat interactions between ion cores and valence electrons.²³ A kinetic energy cutoff of 450 eV

and dense k-point with a grid density of $2\pi \times 0.02 \text{ \AA}^{-1}$ (Monkhorst–Pack scheme)²⁴ are used (an even denser grid of $50 \times 50 \times 1$ is also adopted to converge the magnetic moment when hole doping is introduced). The exchange-correlation potential is incorporated using the PBE²⁵ functional in most cases, while the HSE06 hybrid functional is used to obtain an accurate band gap.^{26,27} The atomic positions are fully relaxed until the total energy converges to 10^{-4} eV and atomic forces are $<10^{-3}$ eV/Å. A large vacuum space of ~ 15 Å in the perpendicular direction is used to eliminate interaction between periodic images. Phonon spectra are obtained using density functional perturbation theory (DFPT)²⁸ implemented in the Quantum ESPRESSO suite (the energy cutoff for the wave function is 60 Ry).²⁹ *Ab Initio* Molecular Dynamics (AIMD) simulations are also performed to confirm the thermal stability. Hole doping is introduced by removing electrons from the unit cell in a jellium background with opposite charge added to maintain charge neutrality, and the atomic positions are reoptimized at different hole densities (in the Supporting

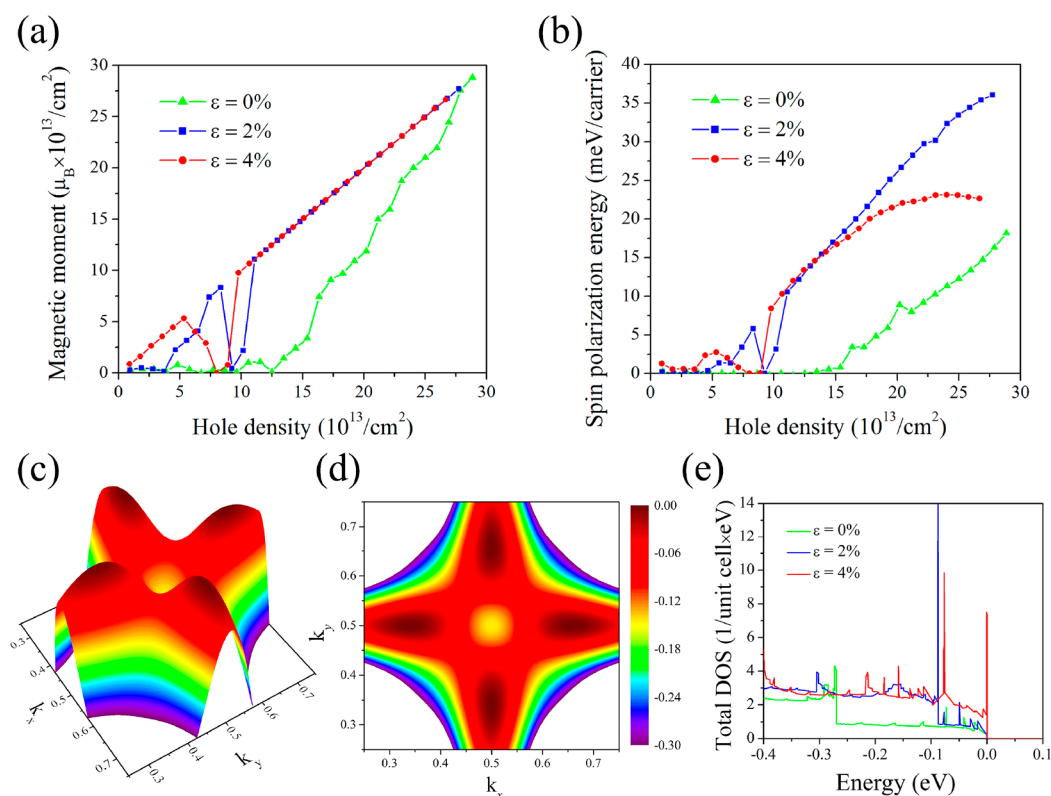


Figure 3. Hole-induced magnetism. (a) Spin moment density vs hole density. (b) Spin polarization energy (PE) per carrier. (c and d) 3D profile and 2D projection of the VBM, respectively, when $\varepsilon = 4\%$. (e) Total DOS of Tetra-MoN₂.

Information, we discuss the validity of our use of VASP to simulate hole-doped Tetra-MoN₂).

RESULTS AND DISCUSSION

Geometry and Stability. Instead of guessing the stable geometry based on chemical knowledge, we resort to a global structure search (CALYPSO) to unveil the ground structure. To our surprise, a new highly stable MoN₂ structure, Tetra-MoN₂, is found, which is much more stable than the previously reported H-MoN₂. As shown in Figure 1a, the new MoN₂ sheet belongs to space group $P\bar{4}M2$ with point group D_{2d} symmetry adopting a highly buckled structure. The optimized lattice constant is $a = b = 3.22$ Å, and the coordination number of Mo in Tetra-MoN₂ is 4 instead of 6 as in H- and T-MoN₂;^{10,13} the Mo–N bond length is 1.88 Å, shorter than the value of 2.02 Å in H- and T-MoN₂.

Then we study the stability of Tetra-MoN₂ with respect to H- and T-MoN₂. First, its dynamical stability is confirmed by calculating the phonon spectra as plotted in panels c and d of Figure S2. Second, the thermal stability of Tetra-MoN₂ over H-MoN₂ is also verified by performing an AIMD simulation at 1000 K as presented in panels a and b of Figure S2, where Tetra-MoN₂ remains intact while the H-MoN₂ sheet disintegrates quickly. Finally, we compare the binding energy per atom for three 2D MoN₂ isomers (H-, T-, and Tetra-MoN₂) and two bulk phases (labeled #1 and #6 in ref 16) as displayed in Figure 1b, from which one can see that bulk phases with more chemical bonds are more energetically favorable (#1, –9.48 eV; #6, –9.23 eV), the Tetra-sheet is next to them with a binding energy of –8.95 eV, and the T and H configurations have higher energies of –8.80 and –8.66 eV, respectively. In Figure 1b, we also plot the energy–area curve for three 2D

isomers, where the eccentric double minimum of the energy–area curve of H-MoN₂ is ascribed to a strain-induced phase transition.¹¹ It is quite interesting to see that the Tetra configuration not only is energetically favored but also has an atom density (defined as the number of atoms per unit area) lower than those of H- and T-MoN₂.

To better understand the results presented above, let us mention the fact that N has fewer valence electrons and a smaller covalent radius than S does, and the geometry of H-MoS₂ would no longer fit the bonding between Mo and N. Actually, in Tetra-MoN₂, strong interactions exist between N p_x and Mo d_{xz} (polarized by Mo p_x) and between N p_y and Mo d_{yz} (polarized by Mo p_y), leading to a short Mo–N bond length of 1.88 Å and a lower total energy due to the strong hybridization between N 2p and Mo 4d as seen in Figure 2b.

Electronic Properties. To study the electronic properties of the Tetra-MoN₂ sheet, we calculate the band structure along high-symmetry lines of the first Brillouin zone (BZ). As presented in Figure 2a, Tetra-MoN₂ is found to be an indirect band gap semiconductor (the VBM is at Γ , and the CBM lies between K and Γ). The solid line shows the results of the calculation using the PBE functional, while the dashed line shows the results for the HSE06 calculation. The band gap is 0.77 eV at the PBE level and increases to 1.41 eV when HSE06 is used. In Figure 2b, the orbital-projected DOS is presented. We can see, because of the difference in electronegativity, that the states near the top of the valence bands are mainly contributed by N p orbitals, while Mo 4d orbitals dominate near the bottom of conduction bands. However, we also observed some covalent bonding features, namely, the sizable DOS of Mo 4d below the Fermi level and the strong 2p–4d orbital hybridization in energy window (–5, –3) eV. This

suggests the mixed covalent and ionic bonding features.³⁰ Because of the localized nature of N p orbitals, the top valence band is relatively flat with a large effective mass. The band-decomposed charge density for the top valence band is plotted in Figure 2c and exhibits exactly the p orbital character of N. The band gap variations of Tetra-MoN₂ with biaxial and uniaxial strain (−5% to 15%) are shown in Figure 2d. The sheet can be tuned either to a metal at 9% biaxial strain or to a semiconductor with a different band gap in uniaxial strain, demonstrating the flexibility in band engineering.

Moreover, the band structures can help us better understand stability. We can see that the semiconducting features in Tetra-MoN₂ and T-MoN₂ result in unoccupied nonbonding and antibonding orbitals, leading to a stable configuration over the metallic H-MoN₂ (resembling the Jahn–Teller effect).

Tunable p-Electron Half-Metallicity and Magnetism.

In general, there are two mechanisms for explaining hole-induced magnetism in 2D or three-dimensional (3D) materials. The first is named the “intrinsic mechanism”, which can be used to understand the intrinsic hole-induced magnetization in some 3D oxides and nitrides.³¹ The requirements for realizing “intrinsic-type” magnetism are (1) a large exchange interaction J and (2) a high DOS near the Fermi level. The second is termed the “DOS-divergent mechanism”, which can be used to understand hole-induced spontaneous ferromagnetism as found in Si₃P₃, PtSe₂, and GaSe (GaS) monolayers where exchange interactions of 3p or 4p orbitals are much weaker.^{32–35} The prerequisite for this mechanism is divergent DOS near the Fermi level. In fact, the two mechanisms mentioned above can be interpreted as different ways of satisfying the “Stoner criterion”: $D_f J > 1$ (D_f is the density of states at the Fermi level, and J is the strength of exchange interaction). We will show that both mechanisms are responsible for hole-induced magnetism in Tetra-MoN₂, but in different doping concentration regions.

On the basis of the relatively flat top valence band and the effective mediation for magnetic coupling of N, we next investigate the possible hole-induced magnetism and relevant applications of Tetra-MoN₂. Because a high carrier density can be achieved experimentally via applying a gate voltage as shown in graphene ($4.0 \times 10^{14} \text{ cm}^{-2}$) and MoS₂ ($2.0 \times 10^{14} \text{ cm}^{-2}$),^{36,37} the carrier concentration studied in our case is confined to $<3.0 \times 10^{14} \text{ cm}^{-2}$. The SOC effect is also negligible and is not included because the top valence bands are mainly composed of N 2p orbitals (Figure S7). Here to quantitatively depict the hole-induced magnetic properties, we calculate the spin moment density and spin polarization energy (PE) per carrier defined as the total energy difference between spin-polarized and unpolarized phases per unit cell normalized by carrier number (the reliability of using this relative energy is discussed in the Supporting Information). The results are shown in panels a and b of Figure 3, respectively, from which one can see that upon continuous injection of more and more holes into relaxed Tetra-MoN₂ ($\epsilon = 0\%$), spin polarization can be induced when the hole density is $>1.25 \times 10^{14} \text{ cm}^{-2}$, and the spin-polarized state becomes the ground state. This phenomenon can be understood via the “intrinsic mechanism” mentioned above. When we increase the hole concentration, the Fermi level moves into the valence band, and the D_f increases accordingly in proportion to $\sqrt{E_{\text{VBM}} - E_f}$, where E_{VBM} and E_f are the energy of VBM and the Fermi level, respectively. When the hole density becomes higher than a

critical value (in our case, $1.25 \times 10^{14} \text{ cm}^{-2}$), the Stoner relation satisfies, namely, $D_f J > 1$, so the sheet turns into a spin-polarized ferromagnetic ground state.

When going further, we can ask the following two questions: Can we reduce the threshold carrier density needed for spontaneous spin polarization? Can we induce the half-metallicity in Tetra-MoN₂? The answers can be based on the tunability of D_f . Although a relatively flat top valence band renders appreciable D_f , only in some extreme cases like van Hove singularity can the DOS be large enough to realize DOS-divergent-type spin polarization. Such a stringent condition was reported in monolayer GaSe and GaS due to the Mexican hat-like dispersion³⁸ in the vicinity of VBM. Fortunately indeed, we find a similar band dispersion near the VBM when the lattice of Tetra-MoN₂ is slightly dilated at the PBE and HSE06 level (Figures S6 and S4), and the biaxial strains needed are lower than the critical strain ($\epsilon = 7\%$) when Tetra-MoN₂ is broken (see Figure S3). In panels c and d of Figure 3, the 3D profile and 2D projection of VBM ($\epsilon = 4\%$) near K (0.5, 0.5) are presented. Shifting from K along different in-plane directions, we would always observe an up and down shaped band dispersion. Because of the lower symmetry, the Mexican hat-like energy surface near the VBM of the strained Tetra-MoN₂ sheet is more anisotropic than that of GaSe or GaS.^{33,34} The underlying mechanism is discussed in Figure S5. The DOS of relaxed and strained Tetra-MoN₂ are plotted in the same figure for comparison in Figure 3e. The divergent behavior of DOS (for $\epsilon = 2\%$ and $\epsilon = 4\%$) that originated from saddle points on the Mexican hat-like energy surface distinguishes itself from the featureless DOS of the relaxed structure.

When the Tetra-MoN₂ sheet is dilated, we find that the spontaneous magnetization is dramatically enhanced with a larger spin moment density and a larger polarization energy per carrier compared to those of relaxed Tetra-MoN₂. As presented in panels a and b of Figure 3, for both $\epsilon = 2\%$ and $\epsilon = 4\%$, Tetra-MoN₂ becomes spin polarized with a large polarization energy; while it becomes half-metallic (straight line in Figure 3a) at both low and high hole concentrations, an attenuated tendency of spin polarization (abrupt dip in the spin moment density) in an intermediate range is observed. This strain-enhanced magnetism can be simply ascribed to a larger DOS with increased strain (largely p orbital-like) near the VBM as presented in Figure 3e. However, the emergence of bizarre dampened magnetism in the intermediate range (off-line curve in Figure 3a of strained cases) needs some explanation. The discussions below are based on $\epsilon = 4\%$ (the $\epsilon = 2\%$ case is similar). As shown in Figure 3a, the strained Tetra-MoN₂ sheet with $\epsilon = 4\%$ becomes half-metallic in both the low-concentration range ($1.0\text{--}5.0 \times 10^{13} \text{ cm}^{-2}$) and the high-concentration range ($1.0\text{--}3.0 \times 10^{14} \text{ cm}^{-2}$). Interestingly, the spin moment density for $\epsilon = 4\%$ undergoes an abrupt dip within the intermediate concentration range ($5.0\text{--}10.0 \times 10^{13} \text{ cm}^{-2}$). We attribute this phenomenon to the different origins of the spontaneous polarization at different doping ranges. The DOS curve for $\epsilon = 4\%$ displayed in Figure 3e shows an apparent peak right below the VBM. Therefore, at low carrier concentrations, the Fermi level becomes slightly lower and moves right into the peak in the DOS curve. Then we have a divergent D_f leading to a spin-polarized state via a “DOS-divergent-type” mechanism. If we increase the doping level further, the Fermi level moves out of the peak in the DOS curve, and D_f would drop dramatically. This is why we observe a dampened magnetism in Tetra-MoN₂ ($\epsilon = 4\%$) in the

intermediate doping range. However, at a high carrier concentration, Tetra-MoN₂ ($\epsilon = 4\%$) becomes half-metallic as the $Df > 1$ relation is satisfied as in the case of 3D oxides (“intrinsic-type” mechanism). Consequently, the “DOS-divergent-type” magnetization is in effect at low doping densities, while “intrinsic-type” magnetism of strained Tetra-MoN₂ plays a role at high doping concentrations. In the intermediate doping level, where both mechanisms fail, Tetra-MoN₂ ($\epsilon = 4\%$) tends to be nonmagnetic.

We summarize the main results in Table 1 by categorizing the spontaneous magnetization under hole doping into “DOS-

Table 1. Summary of the Magnetic Properties of Tetra-MoN₂ (FM, ferromagnetic; HM, half-metallic)

strain	DOS-divergent type	intrinsic type
$\epsilon = 0\%$	none	$>12.5 \times 10^{13} \text{ cm}^{-2}$ (FM)
$\epsilon = 2\%$	$7.0\text{--}9.0 \times 10^{13} \text{ cm}^{-2}$ (HM)	$>11.0 \times 10^{13} \text{ cm}^{-2}$ (HM)
$\epsilon = 4\%$	2.0×10^{12} to $6.0 \times 10^{13} \text{ cm}^{-2}$ (HM)	$>9.0 \times 10^{13} \text{ cm}^{-2}$ (HM)

divergent-type” and “intrinsic-type”. For Tetra-MoN₂ under 4% strain, we further confirmed that a hole concentration as low as $2.0 \times 10^{12} \text{ cm}^{-2}$ is sufficient for complete spin polarization. To visualize the hole-induced half-metallicity in strained Tetra-MoN₂, we plot the spin-resolved band structure and spin charge density distribution in Figure 4 ($\epsilon = 4\%$ and a hole

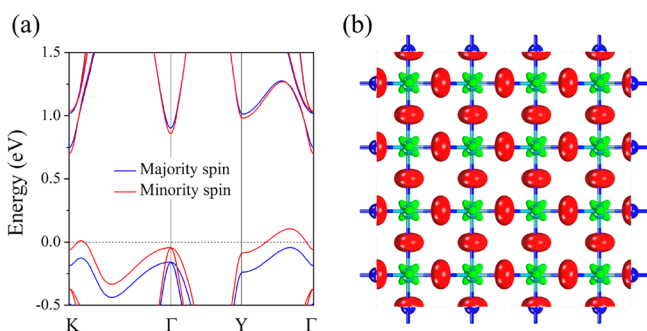


Figure 4. Magnetic properties of Tetra-MoN₂ at $\epsilon = 4\%$ strain and a hole concentration of $1.0 \times 10^{14} \text{ cm}^{-2}$. (a) Spin-resolved band structure. (b) Spin charge density distribution with an isovalue of 0.013 \AA^3 .

density of $1.0 \times 10^{14} \text{ cm}^{-2}$). The splitting of the top valence band, in Figure 4a, is around 100–150 meV. The consequence of this strong exchange splitting is that the Fermi energy intersects with only the minority-spin band, and thus fully polarized spin transport. The spin charge density distribution in Figure 4b shows that spin moments mainly come from polarized p electrons of N with some contributions from d orbitals of Mo. The localized moments on N and Mo are 0.06 and $-0.048 \mu_B$, respectively, while the remaining $0.038 \mu_B$ is distributed in the interstitial space (total moment of $0.11 \mu_B$).

It is worth noting that this is the first example of hole-induced “DOS-divergent-type” and “intrinsic-type” magnetism in a single material but at different carrier densities, and importantly, the applied strain and doping level that are required (as low as $\sim 10^{12} \text{ cm}^{-2}$) are experimentally feasible. While other 2D materials with only “DOS-divergent-type” magnetism generally become spin-polarized at a lower doping level ($\sim 10^{13} \text{ cm}^{-2}$), their magnetism is quenched by surplus carriers ($\sim 10^{14} \text{ cm}^{-2}$).^{32–34} Therefore, the studied Tetra-MoN₂ sheet is quite special in terms of magnetism.

SUMMARY

Motivated by the controversies about the stability of the H-MoN₂ sheet, we have performed a global structure search and identified the ground state geometry, Tetra-MoN₂, which is energetically more stable than the previously proposed H- and T-MoN₂ structures, exhibiting a semiconducting nature instead of metallicity as found in the H-MoS₂ phase. This can be easily understood. Because N has one fewer electron than S does, in the stable H-MoS₂ phase when all S atoms are replaced with N, due to the unfilled electronic orbitals, the resulting Jahn–Teller distortion may cause a structural transition from the H phase to the other, as we found the metallic H phase changes to the semiconducting Tetra phase. Intriguingly, p-electron half-metallicity can be induced readily by synergistically using strain and uniform p-type doping, even at a hole concentration as low as 10^{12} cm^{-2} at $\epsilon = 4\%$. This kind of half-metallicity is absent in the pristine H-MoS₂ sheet without vacancies or impurities. Our study clearly indicates that the MoN₂ sheet has a geometry and properties that are different from those of the MoS₂ sheet and that caution is needed for other metal dinitride sheets, and further studies are highly desirable as these sheets have been explored much less vigorously than transition metal dichalcogenides sheets have been.

ASSOCIATED CONTENT

Supporting Information

The Supporting Information is available free of charge on the ACS Publications website at DOI: [10.1021/acs.chemmater.7b01606](https://doi.org/10.1021/acs.chemmater.7b01606).

Total energy in VASP for charged systems (Table S1 and Figure S1), structural stability (Figure S2), critical strain (Figure S3), band evolution (Figure S4), bonding analysis (Figure S5), HSE06 versus PBE band (Figure S6), and SOC band (Figure S7) (PDF)

AUTHOR INFORMATION

Corresponding Author

*E-mail: sunqiang@pku.edu.cn.

ORCID

Cunzhi Zhang: [0000-0002-4562-535X](https://orcid.org/0000-0002-4562-535X)

Haoming Shen: [0000-0001-7715-9739](https://orcid.org/0000-0001-7715-9739)

Notes

The authors declare no competing financial interest.

ACKNOWLEDGMENTS

This work is partially supported by grants from the National Natural Science Foundation of China (NSFC-21573008) and from the Ministry of Science and Technology of China (2017YFA0204902).

REFERENCES

- (1) Novoselov, K. S.; Geim, A. K.; Morozov, S. V.; Jiang, D.; Zhang, Y.; Dubonos, S. V.; Grigorieva, I. V.; Firsov, A. A. Electric Field Effect in Atomically Thin Carbon Films. *Science* **2004**, *306*, 666–669.
- (2) Cahangirov, S.; Topsakal, M.; Aktürk, E.; Şahin, H.; Ciraci, S. Two- and one-dimensional honeycomb structures of silicon and germanium. *Phys. Rev. Lett.* **2009**, *102*, 236804.
- (3) Fleurence, A.; Friedlein, R.; Ozaki, T.; Kawai, H.; Wang, Y.; Yamada-Takamura, Y. Experimental evidence for epitaxial silicene on diboride thin films. *Phys. Rev. Lett.* **2012**, *108*, 245501.

- (4) Mak, K. F.; Lee, C.; Hone, J.; Shan, J.; Heinz, T. F. Atomically thin MoS_2 : a new direct-gap semiconductor. *Phys. Rev. Lett.* **2010**, *105*, 136805.
- (5) Xu, M.; Liang, T.; Shi, M.; Chen, H. Graphene-like two-dimensional materials. *Chem. Rev.* **2013**, *113*, 3766–3798.
- (6) Li, L.; Yu, Y.; Ye, G. J.; Ge, Q.; Ou, X.; Wu, H.; Feng, D.; Chen, X. H.; Zhang, Y. Black phosphorus field-effect transistors. *Nat. Nanotechnol.* **2014**, *9*, 372–377.
- (7) Liu, H.; Neal, A. T.; Zhu, Z.; Luo, Z.; Xu, X.; Tománek, D.; Ye, P. D. Phosphorene: an unexplored 2D semiconductor with a high hole mobility. *ACS Nano* **2014**, *8*, 4033–4041.
- (8) Zhang, C.; Sun, Q. A Honeycomb BeN_2 Sheet with a Desirable Direct Band Gap and High Carrier Mobility. *J. Phys. Chem. Lett.* **2016**, *7*, 2664–2670.
- (9) Wang, S.; Ge, H.; Sun, S.; Zhang, J.; Liu, F.; Wen, X.; Yu, X.; Wang, L.; Zhang, Y.; Xu, H.; et al. A new molybdenum nitride catalyst with rhombohedral MoS_2 structure for hydrogenation applications. *J. Am. Chem. Soc.* **2015**, *137*, 4815–4822.
- (10) Wu, F.; Huang, C.; Wu, H.; Lee, C.; Deng, K.; Kan, E.; Jena, P. Atomically Thin Transition-Metal Dinitrides: High-Temperature Ferromagnetism and Half-Metallicity. *Nano Lett.* **2015**, *15*, 8277–8281.
- (11) Wang, Y.; Wang, S. S.; Lu, Y.; Jiang, J.; Yang, S. A. Strain-Induced Isostructural and Magnetic Phase Transitions in Monolayer MoN_2 . *Nano Lett.* **2016**, *16*, 4576–4582.
- (12) Zhang, X.; Yu, Z.; Wang, S.-S.; Guan, S.; Yang, H. Y.; Yao, Y.; Yang, S. A. Theoretical prediction of MoN_2 monolayer as a high capacity electrode material for metal ion batteries. *J. Mater. Chem. A* **2016**, *4*, 15224–15231.
- (13) Wu, H.; Qian, Y.; Lu, R.; Tan, W. A theoretical study on the electronic property of a new two-dimensional material molybdenum dinitride. *Phys. Lett. A* **2016**, *380*, 768–772.
- (14) Liu, Z.; Liu, J.; Zhao, J. YN_2 monolayer: Novel p-state Dirac half metal for high-speed spintronics. *Nano Res.* **2017**, *10*, 1972–1979.
- (15) Gong, S.; Zhang, C.; Wang, S.; Wang, Q. Ground-State Structure of YN_2 Monolayer Identified by Global Search. *J. Phys. Chem. C* **2017**, *121*, 10258–10264.
- (16) Yu, S.; Huang, B.; Jia, X.; Zeng, Q.; Oganov, A. R.; Zhang, L.; Frapper, G. Exploring the Real Ground-State Structures of Molybdenum Dinitride. *J. Phys. Chem. C* **2016**, *120*, 11060–11067.
- (17) Wang, Y.; Ding, Y. The hydrogen-induced structural stability and promising electronic properties of molybdenum and tungsten dinitride nanosheets: a first-principles study. *J. Mater. Chem. C* **2016**, *4*, 7485–7493.
- (18) Wang, Y.; Lv, J.; Zhu, L.; Ma, Y. Crystal structure prediction via particle-swarm optimization. *Phys. Rev. B: Condens. Matter Mater. Phys.* **2010**, *82*, 094116.
- (19) Rao, B.; Jena, P. Giant magnetic moments of nitrogen-doped Mn clusters and their relevance to ferromagnetism in Mn-doped GaN. *Phys. Rev. Lett.* **2002**, *89*, 185504.
- (20) Mejía-López, J.; Pinto, J.; Romero, A. Effect of sulphur doping on manganese clusters: an ab initio study. *Eur. Phys. J. D* **2008**, *50*, 45–52.
- (21) Liu, J.; Sun, Q. Enhanced ferromagnetism in a $\text{Mn}_3\text{C}_{12}\text{N}_{12}\text{H}_{12}$ sheet. *ChemPhysChem* **2015**, *16*, 614–620.
- (22) Kresse, G.; Furthmüller, J. Efficient iterative schemes for ab initio total-energy calculations using a plane-wave basis set. *Phys. Rev. B: Condens. Matter Mater. Phys.* **1996**, *54*, 11169–11186.
- (23) Blöchl, P. E. Projector augmented-wave method. *Phys. Rev. B: Condens. Matter Mater. Phys.* **1994**, *50*, 17953–17979.
- (24) Monkhorst, H. J.; Pack, J. D. Special points for Brillouin-zone integrations. *Phys. Rev. B* **1976**, *13*, 5188.
- (25) Perdew, J. P.; Burke, K.; Ernzerhof, M. Generalized gradient approximation made simple. *Phys. Rev. Lett.* **1996**, *77*, 3865–3868.
- (26) Heyd, J.; Scuseria, G. E.; Ernzerhof, M. Hybrid functionals based on a screened Coulomb potential. *J. Chem. Phys.* **2003**, *118*, 8207–8215.
- (27) Heyd, J.; Scuseria, G. E.; Ernzerhof, M. Erratum: “Hybrid functionals based on a screened Coulomb potential. *J. Chem. Phys.* **2006**, *124*, 219906.
- (28) Baroni, S.; De Gironcoli, S.; Dal Corso, A.; Giannozzi, P. Phonons and related crystal properties from density-functional perturbation theory. *Rev. Mod. Phys.* **2001**, *73*, 515.
- (29) Giannozzi, P.; Baroni, S.; Bonini, N.; Calandra, M.; Car, R.; Cavazzoni, C.; Ceresoli, D.; Chiarotti, G. L.; Cococcioni, M.; Dabo, I.; et al. QUANTUM ESPRESSO: a modular and open-source software project for quantum simulations of materials. *J. Phys.: Condens. Matter* **2009**, *21*, 395502.
- (30) Zakutayev, A. Design of nitride semiconductors for solar energy conversion. *J. Mater. Chem. A* **2016**, *4*, 6742–6754.
- (31) Peng, H.; Xiang, H. J.; Wei, S. H.; Li, S. S.; Xia, J. B.; Li, J. Origin and enhancement of hole-induced ferromagnetism in first-row d0 semiconductors. *Phys. Rev. Lett.* **2009**, *102*, 017201.
- (32) Huang, B.; Zhuang, H. L.; Yoon, M.; Sumpster, B. G.; Wei, S.-H. Highly stable two-dimensional silicon phosphides: Different stoichiometries and exotic electronic properties. *Phys. Rev. B: Condens. Matter Mater. Phys.* **2015**, *91*, 121401.
- (33) Cao, T.; Li, Z.; Louie, S. G. Tunable Magnetism and Half-Metallicity in Hole-Doped Monolayer GaSe. *Phys. Rev. Lett.* **2015**, *114*, 236602.
- (34) Wu, S.; Dai, X.; Yu, H.; Fan, H.; Hu, J.; Yao, W. Magnetisms in p-type monolayer gallium chalcogenides (GaSe , GaS). *arXiv preprint* **2014**, 1409.4733.
- (35) Zulfikar, M.; Zhao, Y.; Li, G.; Nazir, S.; Ni, J. Tunable Conductivity and Half Metallic Ferromagnetism in Monolayer Platinum Diselenide: A First-Principles Study. *J. Phys. Chem. C* **2016**, *120*, 25030–25036.
- (36) Efetov, D. K.; Kim, P. Controlling electron-phonon interactions in graphene at ultrahigh carrier densities. *Phys. Rev. Lett.* **2010**, *105*, 256805.
- (37) Ye, J.; Zhang, Y.; Akashi, R.; Bahramy, M.; Arita, R.; Iwasa, Y. Superconducting dome in a gate-tuned band insulator. *Science* **2012**, *338*, 1193–1196.
- (38) Li, X.; Lin, M. W.; Puzos, A. A.; Idrobo, J. C.; Ma, C.; Chi, M.; Yoon, M.; Rouleau, C. M.; Kravchenko, I. I.; Geoghegan, D. B.; Xiao, K. Controlled vapor phase growth of single crystalline, two-dimensional GaSe crystals with high photoresponse. *Sci. Rep.* **2015**, *4*, 5497.